# Responses to SSM on Hydrogeology

## Lee Hartley and Steve Joyce, AMEC, 23rd May 2013

### Question 1

A response will be prepared to this question by December 2013.

### Question 2

The properties of each finite-element (piecewise constant within an element) have been exported for ECPM simulation of the so-called Base Case Hydro DFN model and collated in the worksheet "SSM-properties-question2.xlsx". The embedded detailed area of the hydrogeological model uses a 20m grid (see Figure 3-6 of R-07-49 (Follin et al. 2007b)) that covers the volumes occupied by FFM01, FFM02 and FFM06 of relevance to the repository layout considered, and so it is important to recognise these properties relate to the 20m scale. The extent of the embedded 20m grid in the ECPM model is shown here in Figure 2-1, along with the distributions of fracture domains. To keep the property export relatively small and accessible, properties are restricted to those elements belonging to FFM01+FFM06 (being the same hydraulic domain) and FFM02, which make up the target volume for SR-Site. The properties of any element cut by a deformation zone are not included as their statistics would be different. Properties for the peripheral fracture domains FFM03-FFM05 could also be exported on request, but these span both the embedded 20m grid area and the surrounding area that uses a 100m grid. Because of the scale dependence of properties, it is only meaningful to calculate statistics on the two scales separately, making the analysis more complex.

Permeability is exported in units of $m^2$ and only in the axial directions; though a full 6-component symmetric tensor is used in the upscaling and ECPM simulations to allow flow in any direction according to connectivity of the underlying fracture system. Permeabilities in $m^2$ are converted to hydraulic conductivity in m/s for purposes of comparison here by simply multiplying by $10^7$ s/m, although a proper evaluation of fluid density and viscosity and gravitational acceleration are used in the solute transport calculations (according to salinity, temperature and pressure). Permeability is calculated by upscaling a Hydro-DFN model that covers the full extent of each fracture domain FFM01-FFM06 (See Figure 2-1 and Figure 3-16 of R-07-49 which gives an example of the generated fractures) with a minimum imposed of $10^{-18}m^2 \sim 10^{-11}$m/s in the ECPM calculations. Some statistics are presented in Table 2-1 for convenience; they may be compared to related statistics for the data and a more comprehensive presentation of modelling results in response to Question 3. There is no distinction of fracture properties within FFM02 by depth, and hence there is little difference between them. Arithmetic means are given as an indication of large scale bulk conductivity, as well as geometric means as an indication of typical values on the 20m scale. $K_e$ is the geometric mean of $K_x$, $K_y$, $K_z$.

**Table 2-1. Statistics of $Log_{10}$(hydraulic conductivity) for the rock inside the target volume outside of deformation zone given as arithmetic ($Log(\overline{K_x})$)and geometric ($\overline{Log(K_x)}$)means of the E-W directional permeability and likewise for the N-S direction (*y*) and the vertical direction (*z*) based on "SSM-properties-question2.xlsx".**

| FFM | z | $Log(\overline{K_x})$ | $\overline{Log(K_x)}$ | $Log(\overline{K_y})$ | $\overline{Log(K_y)}$ | $Log(\overline{K_z})$ | $\overline{Log(K_z)}$ | $\overline{Log(K_e)}$ |
|---|---|---|---|---|---|---|---|---|
| 02 | >-200m | -7.1 | -8.1 | -7.0 | -8.1 | -8.5 | -9.4 | -8.5 |
| 02 | <-200m | -7.2 | -8.3 | -6.9 | -8.3 | -8.3 | -9.4 | -8.7 |
| 01+06 | >-200m | -6.3 | -8.1 | -6.3 | -8.1 | -8.0 | -9.4 | -8.5 |
| 01+06 | -200m to -400m | -8.1 | -9.7 | -8.1 | -9.6 | -9.4 | -10.5 | -9.9 |
| 01+06 | <-400m | -9.8 | -10.8 | -9.7 | -10.8 | -9.7 | -10.8 | -10.8 |

Kinematic porosity is calculated by upscaling the Hydro-DFN model of the fracture domains (only the connected open fracture volume is considered). This can be sensitive to the minimum fracture size used in the fracture generation. A fracture size truncation of 5.68m radius was used throughout the fracture domain volumes in generating the Base Case Hydro-DFN, with smaller fractures only generated in a volume surrounding the repository. Sensitivity tests of including fractures down to c. 1m typically lead to a kinematic porosity of a factor c. 2 times higher. The sensitivity of the evolution of groundwater composition due to changes in palaeo-climate was tested as part of the SDM confirmatory tests (see Section 6 of R-07-49, for example). The composition evolution was found to be moderately sensitive to kinematic porosity if order of magnitude changes (i.e. factor 10) were made, i.e. changes had to be made much larger than the sensitivity to fracture truncation in order to see a significant effect. Hence, consequences of the fracture size truncation on the calculations of groundwater evolution are not expected to be significant. It may, however, have a significant effect if it were used to calculate travel times for non-sorbing solutes in the absence of rock matrix diffusion.

It is noted that kinematic porosity calculated in this way is sensitive to uncertainties in the relationship assumed between fracture transmissivity and aperture, and hence relates to Question 4. The kinematic porosity calculated by upscaling is spatially varying, and was used in both transient solute transport calculations, and in estimated travel times in the ECPM model, although such ECPM based estimates were generally not used in SR-Site.

Flow wetted surface (per volume of rock) was also calculated by upscaling the Hydro-DFN of the fracture domains (only the connected open fracture volume is considered), and can be sensitive to the minimum fracture size used in the fracture generation (at least in the more connected upper parts of the bedrock). This is calculated for each element of volume, $V$, as

$$a_{rf} = 2P_{32} = 2\sum_f {A_f}/{V}\,, \qquad (2\text{-}1)$$

where the sum is over each fracture, $f$, inside or cutting part of the volume with area $A_f$ inside the volume, and $P_{32}$ is the fracture surface area per unit volume. The

evolution of groundwater composition due to changes in palaeo-climate was found to have significant sensitivity to flow wetted surface in the SDM confirmatory tests (see Section 6 of R-07-49) as it controls the magnitude of solute flux exchange between fractures and matrix. In the SDM it was parameterised as a piecewise constant parameter within each hydraulic domain (fracture domain, subdivided according to depth), estimated from the frequency of PFL detected fractures, and considered as a calibration parameter in confirmatory tests of palaeo-climate. The same approach was used in SR-Site, but the parameterisation defined more consistently with data (see Table C-2, R-09-20). The element specific values based on upscaling the Hydro-DFN model are given in the spreadsheet. Statistics for solute transport parameters are given in Table 3-2, where $\phi_f$ and $a_{rf}$ are the kinematic porosity and flow wetted surface, respectively, calculated from the regional Hydro-DFN. Statictics of $a_{rf}$ are given in Column L (logarithm of arithmetic mean) and Column M (geometric mean) of the file "SSM-properties-question2.xlsx". $a_r$ is the flow wetted surface estimated from the measured frequency of PFL detected fractures (see Column N of "SSM-properties-question2.xlsx"):

$$a_r = 2P_{10,PFL,corr}, \tag{2-2}$$

It is seen that below -200m the modelled flow wetted surface is similar to that estimated from measurements (see Table 10-21 through Table 10-24 of R-07-48 (Follin et al. 2007a), for $P_{10,PFL,corr}$ – corrected intensity of PFL fractures ). This is because the fracture network is sparse at such depths such that the fractures below the size truncation used in generating the fracture network would in that case not be connected, and so not contributing to the modelled flow wetted surface. Above -200m the fracture network is more connected and so truncating the fracture size distribution does give a lower modelled flow wetted surface than estimated from the PFL frequency.

**Table 2-2. Statistics of $Log_{10}$(kinematic porosity) and $Log_{10}$(flow wetted surface) for the rock inside the target volume outside of deformation zone given as arithmetic and geometric means based on "SSM-properties-question2.xlsx".**

| FFM | z | $Log(\overline{\phi_f})$ | $\overline{Log(\phi_f)}$ | $Log(\overline{a_{rf}})$ | $\overline{Log(a_{rf})}$ | $Log(a_r)$ |
|---|---|---|---|---|---|---|
| 02 | >-200m | -3.5 | -3.7 | -0.6 | -0.8 | -0.2 |
| 02 | <-200m | -3.5 | -3.8 | -0.7 | -0.8 | -0.2 |
| 01+06 | >-200m | -3.2 | -3.6 | -0.8 | -1.1 | -0.5 |
| 01+06 | -200m to -400m | -4.1 | -4.2 | -0.9 | -1.2 | -1.1 |
| 01+06 | <-400m | -4.3 | -4.3 | -1.2 | -1.6 | -1.7 |

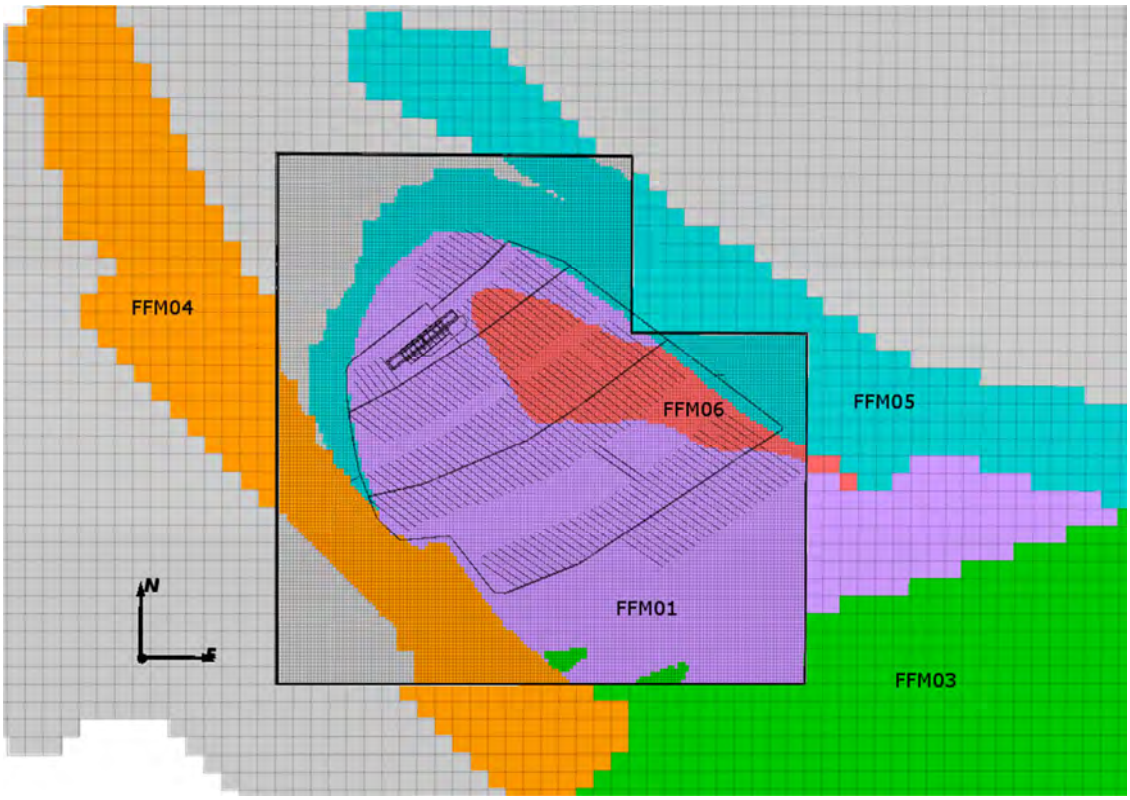


***Figure 2-1.*** *Extent of the embedded 20m grid and the distribution of fracture domains at -470m as implemented in the hydrogeological base case model. The central L shaped area is the region for which properties have been exported. FFM02 lies above FFM01 and FFM06. The repository layout is superimposed for context.*

**Question 3**

We interpret this question as broadly requesting estimates of bulk hydraulic conductivity of the rock within the target volume. Because it is observed at the site that geological structures exist on a range of scales from metres to several kilometres, then there is little basis for expecting that statistics of hydraulic conductivity become stable at any particular scale. Therefore, hydraulic properties are scale dependent, and the concept of a representative elementary volume (REV) has no clear relevance to the hydrogeological description of Forsmark. On a horizontal plane within a block of scale 500m within the target volume there are typically several deformation zones (see Figure 3-4; R-07-48) that would be expected to dominate the hydraulic conductivity on that scale. The effective conductivity of such a 500m block would largely depend on which deformation zones were located within the block (see Table 8-1; R-07-48, for example). In a vertical plane, hydraulic conductivity reduces by about three orders of magnitude over the top 500m of bedrock. This is true for the transmissivity of deformation zones (see Figure 9-1; R-07-48), the maximum transmissivity of fractures in the rock mass in the target rock domain FFM01 (compare Max T in Table 10-22, 10-23 and 10-24; R-07-48), and the arithmetic average effective conductivity of the rock mass in the target rock domain FFM01 (compare ∑T-PFL/∑length in Table 10-22, 10-23 and 10-24; R-07-48; see tables below). It is therefore difficult to capture such important hydrogeological structural characteristics of the rock in any “averaged” properties on the scale of

500m. Instead we focus here on calculating various estimates of effective hydraulic conductivity of the fracture domains FFM01-FFM06 (the rock mass between the deformation zones), with FFM01 and FFM06 being of most importance to the target volume. For the data, averages are considered by collating hydraulic measurement of individual fractures or 5m intervals aggregated over the borehole intervals sampled for each fracture domain typically c. 100m-3km in total for an individual domain. For model properties, upscaled block properties are considered for the 20m scale as used in the site scale sub-region of the hydrogeological model (see Figure 3-6 of R-07-49). In comparing such statistics it should be recognised that data is being collated in terms of flows under pumping conditions to a borehole (PFL) or injection from a borehole (PSS), while upscaled properties are considering flow through a cuboid volume.

**Estimates based on data**

One simple estimate of effective hydraulic conductivity available from the PFL hydraulic tests is the arithmetic sum of transmissivity of all PFL detected fractures divided by the total borehole length in which measurements were made

$$K_{ea} = \sum T \Big/ \sum L \tag{3-1}$$

Such an average can be dominated by any single high values measured, and so if there are a few abnormally high values within several kilometres of measurements, then this average would be an over-estimate of the median conductivity for blocks of c. 100m.

Other possible estimates of average conductivity can be calculated from the intensity of PFL detected fractures ($P_{10,PFL,corr}$ – i.e. corrected for orientation of the borehole) and the geometric mean transmissivity of these fractures:

$$K_{eg} = P_{10\,PFL,corr} \times 10^{\overline{Log(T)}} \tag{3-2}$$

Note: calculating the arithmetic mean transmissivity from the geometric mean transmissivity and standard deviation as $\overline{T} = \exp(\overline{\ln(T)} + \sigma(\ln(T))^2 / 2)$ and multiplying by $P_{10,PFL,corr}$ gives similar results to Eq (3-1).

These formulae are used to estimate hydraulic conductivity from the statistics of PFL data available in R-07-48 as presented in Table 3-1. It is seen that the arithmetic means compared well with the block horizontal conductivities given in Table 2-1, within half an order of magnitude, for domains in the target volume, as do the geometric means.

**Table 3-1. Arithmetic mean and geometric mean estimates of $Log_{10}$(hydraulic conductivity) for the rock inside the target volume outside of deformation zone based on measured PFL hydraulic test data.**

| FFM | z | *Length* $\sum L$ | $P_{10,PFL,corr}$ | $\sum T$ | $\overline{Log(T)}$ | $Log(K_{ea})$ | $Log(K_{eg})$ | References in R-07-48 |
|---|---|---|---|---|---|---|---|---|
| 02 | - | 366 | 0.326 | $1.56 \cdot 10^{-5}$ | -8.0 | -7.4 | -8.5 | Tables 10-16, 10-25 |
| 01+06 | >-200m | 474 | 0.152 | $6.83 \cdot 10^{-5}$ | -7.8 | -6.8 | -8.7 | Tables 10-16, 10-25 |
| 01+06 | -200m to -400m | 1388 | 0.042 | $7.19 \cdot 10^{-7}$ | -8.5 | -9.3 | -9.9 | Tables 10-16, 10-25 |
| 01+06 | <-400m | 3280 | 0.005 | $2.07 \cdot 10^{-7}$ | -8.2 | -10.2 | -10.5 | Tables 10-16, 10-25 |
| 03 | | 1334 | 0.072 | $2.15 \cdot 10^{-6}$ | | -8.8 | | Table 10-17 |
| 04 | | 155 | 0.152 | $1.15 \cdot 10^{-6}$ | | -8.1 | | Table 10-18 |
| 05 | | 122 | 0.027 | $4.00 \cdot 10^{-7}$ | | -8.5 | | Table 10-19 |

Estimates can also be made from 5m PSS hydraulic data given in Tables 5-2, 5-6, 5-7, 5-10, 5-11, 5-13, 5-16, 5-18, and 5-19 of R-07-48 as given in Table 3-2. Here, the geometric mean is calculated simply as the geometric mean of $\sum T/\sum L$ for each reported borehole interval. In considering these estimates it should be noted that only borehole intervals allowing injection above the detection limit of the 100m and then 20m scale were tested on the 5m scale, so that tight intervals were not tested on the 5m scale, and hence the values given represent a biased sample of the more conductive intervals. The PSS intervals also typically cover a smaller overall length of boreholes. Nevertheless, the values reflect characteristics seen in the PFL data of a c. three orders of magnitude decrease in conductivity with depth in FFM01, and about one order of magnitude difference between arithmetic and geometric means. Some PSS tests were performed in more conductive near surface intervals than measured in the PFL tests. This is the cause for the higher mean conductivities given for FFM02.

**Table 3-2. Arithmetic and geometric mean estimates of $Log_{10}$(hydraulic conductivity) for the rock inside the target volume outside of deformation zone based on measured 5m PSS hydraulic test data.**

| FFM | z | *Length* $\sum L$ | $\sum T$ | $Log(K_{ea})$ | $Log(K_{eg})$ |
|---|---|---|---|---|---|
| 02 | - | 270 | $4.79 \cdot 10^{-4}$ | -5.8 | -6.9 |
| 01+06 | >-200m | 418 | $3.10 \cdot 10^{-5}$ | -7.1 | -8.0 |
| 01+06 | -200m to -400m | 283 | $3.52 \cdot 10^{-6}$ | -7.9 | -9.2 |
| 01+06 | <-400m | 681 | $1.51 \cdot 10^{-7}$ | -9.7 | -10.0 |
| 03 | >-100m | 67 | $4.28 \cdot 10^{-6}$ | -7.2 | -7.4 |
| 04 | >-400m | 142 | $1.15 \cdot 10^{-6}$ | -8.1 | -8.2 |
| 04 | <-400m | 195 | $4.29 \cdot 10^{-8}$ | -9.7 | -9.3 |
| 05 | | 195 | $1.47 \cdot 10^{-8}$ | -9.7 | -9.7 |

### Estimates based on DFN modelling

As part of QA checking of the upscaled properties for each realisation of the Hydro-DFN model of fracture domains generated for SR-Site (R-09-20), a java script was used to calculate the mean and standard deviation in the logarithm of the effective hydraulic conductivity for all 20m elements that were conductive. Those results are also reported here for the hydrogeological base case model, as they offer some

different statistics on modelled conductivities that may be of interest. Here, the effective conductivity was calculated as the geometric mean of the eigenvalues of the symmetric conductivity tensor. Elements were judged to be conductive if they had three non-zero eigenvalues, implying the network connected most faces of the element. The percentage of conductive elements, geometric mean conductivity and standard deviation are given in Table 3-3. These results are based on the same DFN model as Table 2-1. Those elements that do not conduct in three dimensions only affect the percentage statistics that are given in Table 3-3. In the ECPM simulations the minimum hydraulic conductivity is set to a value of $10^{-11}$ m/s, which is reflected in the statistics given in Table 2-1. Also, Table 3-3 is based on an analysis of the full six component symmetric tensor (where the principal components are non-zero) rather than just the 3 axial components as presented in Table 2-1. It is seen that results are similar to the geometric mean calculated in Table 2-1; slightly higher due to the exclusion of non-conductive elements. Properties for the additional fracture domains FFM03-FFM05 are also included here where they are represented on a 20m scale. These domains are interpreted as having a weaker depth trend and of higher hydraulic conductivity at depth.

Hence, here we calculate 3 eigenvalues of the symmetric tensor: $K_1$, $K_2$, $K_3$. If $K_3>0$, we calculate

$$\log(K_e) = (\log(K_1) + \log(K_2) + \log(K_3)) \qquad (3\text{-}3)$$

The percentage of elements for which $K_3>0$ is calculated (third column of Table 3-3) and the mean and standard deviation of $\log(K_e)$ over those elements for which $K_3>0$.

**Table 3-3. Statistics of $Log_{10}$(effective hydraulic conductivity) for 20m elements in the base case hydrogeological model for the rock inside the target volume outside of deformation zone based on measured PFL hydraulic test data.**

| FFM | z | *% elements conductive* | $\overline{Log(K_e)}$ | $\sigma(\log(K_e))$ |
|---|---|---|---|---|
| 02 | - | 97 | -8.2 | 0.8 |
| 01+06 | >-200m | 86 | -7.8 | 1.1 |
| 01+06 | -200m to -400m | 78 | -9.4 | 1.0 |
| 01+06 | <-400m | 29 | -10.7 | 1.0 |
| 03 | >-400m | 80 | -8.9 | 0.9 |
| 03 | <-400m | 61 | -9.2 | 0.9 |
| 04 | >-400m | 83 | -8.6 | 0.9 |
| 04 | <-400m | 68 | -8.7 | 0.7 |
| 05 | >-400m | 85 | -8.7 | 0.9 |
| 05 | <-400m | 61 | -9.1 | 0.7 |

ECPM properties calculated by upscaling the Forsmark Hydro-DFN model for cuboid blocks of fixed scale of 5m, 20m and 100m have been calculated. The results are presented graphically here in Figure 3-1 for FFM01/06. It has to be noted that in this case the effective hydraulic conductivity is calculated for each fracture domain and depth in isolation, and so the upscaled properties are not calculated in the structural context of the more conductive volumes above or surrounding FFM01/06 or deformation zones that can produce more conductive fractures or connected fractures protruding into FFM01/06. This overlap of depth zones was intrinsic in the modelling approach used in the calibration of the Hydro-DFN model, and also in the

site DFN model of the fracture domains presented in Tables 2-1 and 3-3. When this overlap is removed, the effective hydraulic conductivity calculated for FFM01/06 below -400m is reduced, as can be seen by comparing the block scale results shown in Figure 3-1 with the numbers given in Table 2-1. In Figure 3-1 the bars compare the geometric mean horizontal hydraulic conductivity calculated by upscaling on 5m, 20m and 100m scales, and the bars show the standard deviation in log(hydraulic conductivity). The modelled values are also scaled by the percentage of active blocks to take account of the significant numbers of blocks for which flow does not percolate through the fracture network. For the PSS data, the values are scaled by the number of intervals with hydraulic conductivity above the detection limit to account for e.g. borehole intervals that were not tested on the 5m scale, because there was no flow detected over the 20m interval spanning that interval. Horizontal hydraulic conductivity is compared with estimates from PFL and PSS data since the vertical component of hydraulic conductivity is not really measured directly in the predominantly vertical boreholes.

Both data and model values show the expected reduction in mean hydraulic conductivity for a reduced length scale, but an increase in variability. The variations in modelled hydraulic conductivities typically span the measured values. Modelled and measured values show reasonable consistency in the upper two depth zones. The upscaled values for the lowest depth zone are lower when this zone is modelled in isolation when compared to both the regional model results given in Table 2-1 and measured values for the reasons described above.

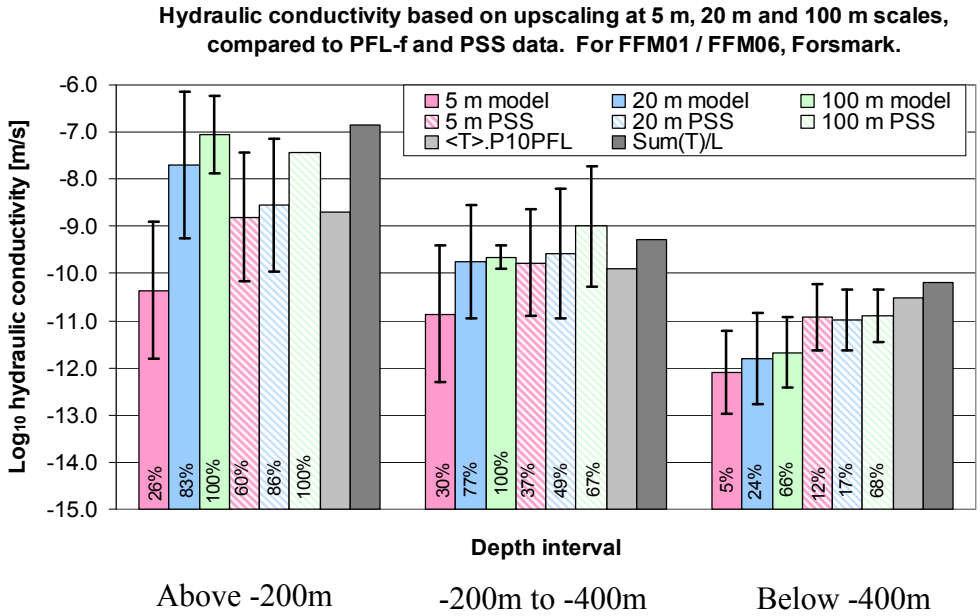


***Figure 3-1.*** *A comparison of upscaled mean horizontal hydraulic conductivities for 5 m, 20 m, and 100 m blocks predicted by the base case DFN model against hydraulic conductivities measured by the PSS method with 5 m, 20 m, and 100 m borehole sections and PFL-f data. The comparison is for FFM01 / FFM06. (Based on parameters from R-07-48, Table 11-20 therein.)*

**Question 4**

Equation (4-20) in Section 4.3.1 of TR-10-66 (SKB 2010b) relates the buffer erosion rate, $R_{Erosion}$ [kg/y], to the water velocity, $v$ [m/y], and the fracture aperture, $\delta$ [m], according to:

$$R_{Erosion} = A_{ero}\delta v^{0.41} \tag{4-1}$$

where the exponent 0.41 and the constant $A_{ero}$ are fitted data from Moreno et al. (2010). As in input to radionuclide transport calculations, the average equivalent flux, $U_{r1}$, for all fractures intersecting a deposition hole is given in Equation (3-8) of R-09-20 (Joyce et al. 2010) as:

$$U_{r1} = \frac{1}{w_c}\sum_f \frac{Q_f}{\sqrt{a_f}} \tag{4-2}$$

where $w_c$ is the canister height [m], $Q_f$ is the volumetric flow rate in the fracture intersecting the deposition hole [m$^3$/y], and $a_f$ is the area of the fracture plane intersecting the deposition hole [m$^2$]. Re-arranging Equation (3-6) of R-09-20 (Joyce et al. 2010) gives the transport velocity, $v$ [m/y], as

$$v = \frac{Q_f}{e_{tf}\sqrt{a_f}} \tag{4-3}$$

where $e_{tf}$ is the transport aperture [m]. Combining Equations (4-2) and (4-3) and neglecting multiple fracture intersections for a deposition hole gives

$$v = \frac{U_{r1}w_c}{e_{tf}} \tag{4-4}$$

Combining Equations (4-1) and (4-4) and equating transport velocity with water velocity and transport aperture with fracture aperture gives

$$R_{Erosion} = A_{ero}e_{tf}\left(\frac{U_{r1}w_c}{e_{tf}}\right)^{0.41} \tag{4-5}$$

The accompanying spreadsheet ("hydrogeological_base_case_r0_velocity.xls") presents the water velocities and erosion rates calculated according to Equation (4-5) from the $U_{r1}$ and $e_{tf}$ values produced from the SR-Site temperate climate simulations for the hydrogeological base case reported in R-09-20 (Joyce et al. 2010), where the $w_c$ value is 5 m. The $e_{tf}$ value calculated by the simulations corresponds to the fracture with the highest groundwater flux that intersects a deposition hole, whereas the $U_{r1}$ value sums the contributions from all of the fractures that intersect the hole. So in the cases where two or more fractures intersect a deposition hole, the $R_{Erosion}$ value would be over-estimated, but such situations are rare and the total flow is likely to be dominated by only one of the intersecting fractures in any case.

Clearly, the calculated rates of erosion are dependent on the transport apertures. For the SR-Site hydrogeological base case, transport aperture is calculated from the fracture transmissivity, $T$, according to the relationship given in Equation (6-1) of

Section 6.2.7 in R-09-20 (Joyce et al. 2010); see also section 5.4.8 in R-09-22 (Selroos and Follin, 2010):

$$e_{tf} = 0.5T^{0.5} \tag{4-6}$$

However, alternative relationships have also been proposed, including one from R-09-28 (Hjerne et al. 2010), based on a compilation of Swedish tracer test data:

$$e_t = 0.28T^{0.3} \tag{4-7}$$

Some of the implications of using this alternative relationship were examined in Section 6.2.7 of R-09-20 (Joyce et al. 2010), where travel times were found to increase due to the decrease in transport velocity resulting from the increase in transport aperture. Equation (4-5) also predicts an increase in erosion rate if the transport aperture is increased as a result of applying the relationship in Equation (4-7) rather than Equation (4-6), as shown in Figure 4-1. However, the relationship from R-09-28 (Hjerne et al. 2010) is based on data that is not specific to the Forsmark site. Possible upper bounds on transport aperture values for Forsmark can be inferred from the volumetric fracture aperture values estimated from borehole data in Appendix A3 of TR-10-52 (SKB 2010a). Note that the volumetric aperture includes the full fracture volume and so is expected to be larger than the transport aperture, which is associated with flowing water only. Figure 4-2 compares the transport apertures calculated from the transmissivities of flow conducting fractures intersecting deposition holes in the hydrogeological base case temperate climate period model using the two relationships. Also shown is the mean volumetric fracture aperture estimated from electrical resistivity measurements taken at Posiva Flow Log (PFL) anomaly locations for boreholes located in the sparsely fractured host rock of the proposed repository volume. An additional line shows the maximum volumetric fracture aperture calculated at PFL anomaly locations for all Forsmark boreholes, including those outside the repository volume. These plots indicate that the SR-Site relationship given in Equation (4-6) is more consistent with the Forsmark site data and so is appropriate for use in calculating erosion rates. The effects of the (Hjerne et al. 2010) relationship for aperture on the extent of erosion at 100,000 years was assessed in SR-Site as a variant case referred to as “Pessimistic fracture aperture” in e.g. Figure 12-3 of TR-11-01 (SKB 2011).

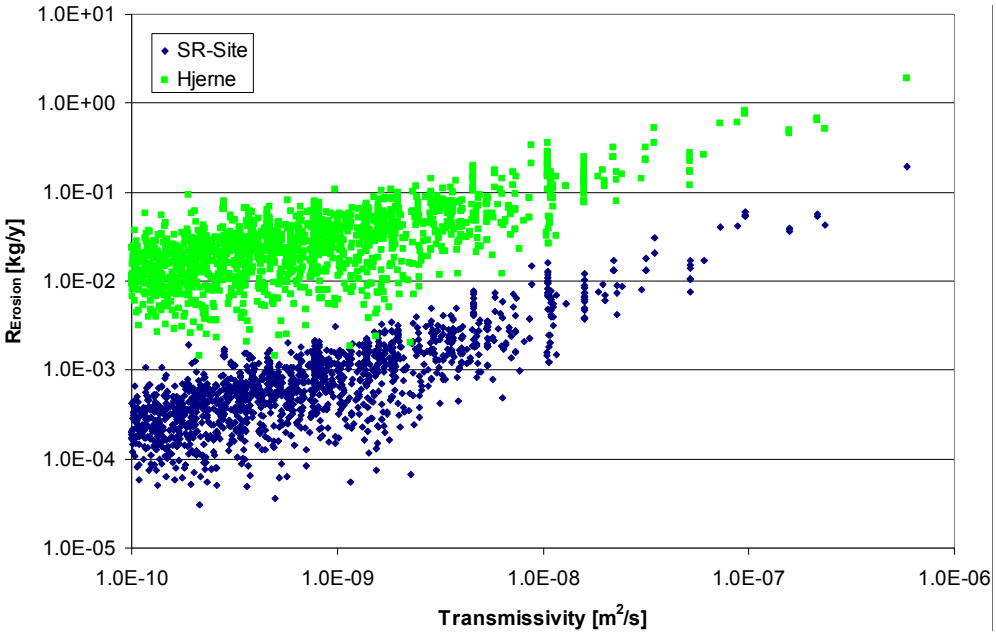


***Figure 4-1.*** *Plots of buffer erosion rate against transmissivity for flow conducting fractures outside of deformation zones intersecting deposition holes in the hydrogeological base case for the temperate climate period at 2000 AD. The transport apertures are calculated according to Equation (4-6) (SR-Site) or Equation (4-7) (Hjerne et al. 2010).*

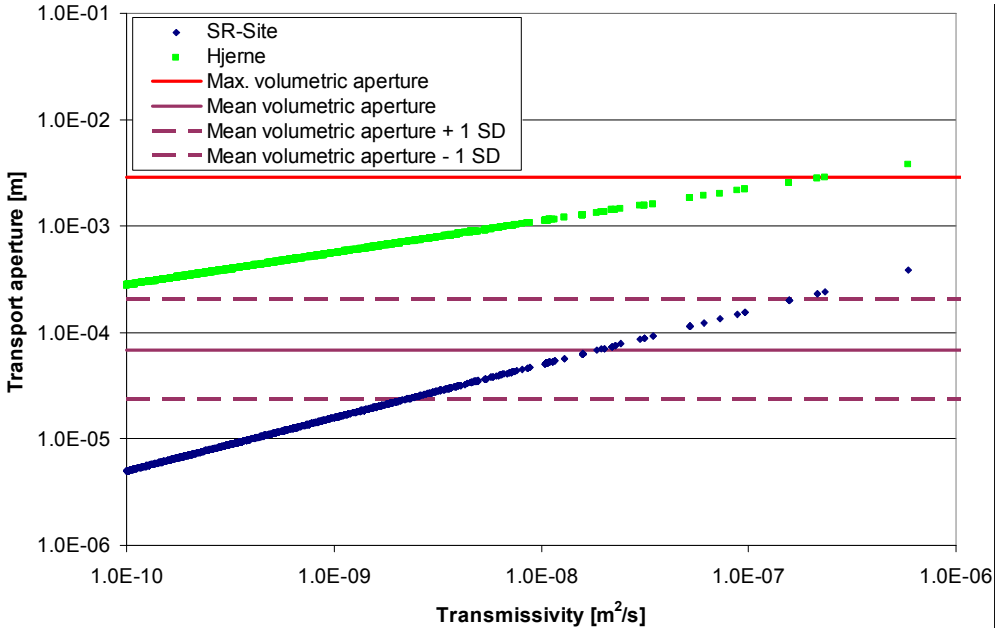


***Figure 4-2.*** *Plots of transport aperture against transmissivity for flow conducting fractures outside of deformation zones intersecting deposition holes in the hydrogeological base case for the temperate climate period at 2000 AD. The transport apertures are calculated according to either Equation (4-6) (SR-Site) or Equation (4-7) (Hjerne et al. 2010). The purple line shows the mean volumetric fracture aperture calculated for boreholes within the Forsmark repository volume, with the dashed lines indicating one standard deviation variation. The red line shows the maximum*

*volumetric fracture aperture calculated for all Forsmark boreholes. Volumetric fracture aperture data was obtained from Appendix A3 in TR-10-52 (SKB 2010a).*

**Question 5**

The buffer erosion calculations depend on the water velocities, as described in TR-10-66 (SKB 2010b) and presented in Equation (4-1) above. The response to Question 4 describes how the average equivalent flux and transport aperture values calculated in R-09-20 (Joyce et al. 2010) can be related to buffer erosion in Equation (4-5). The buffer erosion and water velocity values calculated for each deposition hole of the hydrogeological base case under temperate climate conditions are presented in the accompanying spreadsheet ("hydrogeological_base_case_r0_velocity.xls").

# References

**Follin S, Levén J, Hartley L, Jackson P, Joyce S, Roberts D, Swift B, 2007a.** Hydrogeological characterisation and modelling of deformation zones and fracture domains, Forsmark modelling stage 2.2. SKB R-07-48, Svensk Kärnbränslehantering AB.

**Follin S, Johansson P-O, Hartley L, Jackson P, Roberts D, Marsic N, 2007b.** Hydrogeological conceptual model development and numerical modelling using CONNECTFLOW, Forsmark modelling stage 2.2. SKB R-07-49, Svensk Kärnbränslehantering AB.

**Hjerne C, Nordqvist R, Harrström J, 2010.** Compilation and analyses of results from cross-hole tracer tests with conservative tracers. SKB R-09-28, Svensk Kärnbränslehantering AB.

**Joyce S, Simpson T, Hartley L, Applegate D, Hoek J, Jackson P, Swan D, Marsic N, Follin S, 2010.** Groundwater flow modelling of periods with temperate climate conditions – Forsmark. SKB R-09-20, Svensk Kärnbränslehantering AB.

**Moreno L, Neretnieks I, Liu L, 2010.** Modelling of erosion of bentonite gel by gel/sol flow. SKB TR-10-64, Svensk Kärnbränslehantering AB.

**Selroos J-O, Follin S, 2010.** SR-Site groundwater flow modelling methodology, setup and results. SKB R-09-22, Svensk Kärnbränslehantering AB.

**SKB, 2010a.** Data report for the safety assessment SR-Site. SKB TR-10-52, Svensk Kärnbränslehantering AB.

**SKB, 2010b.** Corrosion calculations report for the safety assessment SR-Site. SKB TR-10-66, Svensk Kärnbränslehantering AB.

**SKB, 2011.** Long-term safety for the final repository for spent nuclear fuel at Forsmark. Main report of the SR-Site project. Volume III. SKB TR-11-01, Svensk Kärnbränslehantering AB.